

Perturbations of the global carbon cycle across the Cretaceous–Palaeogene boundary

Mingming Ma

mamingming159@163.com

Fujian Normal University <https://orcid.org/0000-0003-4896-6886>

Mengdi Wang

Fujian Normal University

Huixin Huang

Fujian Normal University

Xiuming Liu

Fujian Normal University

Article

Keywords: Terrestrial record, Cretaceous-Palaeogene boundary, Global carbon cycle, Deccan Traps, Orbital forcing

Posted Date: February 8th, 2024

DOI: <https://doi.org/10.21203/rs.3.rs-3893195/v1>

License:  This work is licensed under a Creative Commons Attribution 4.0 International License.

[Read Full License](#)

Additional Declarations: There is **NO** Competing Interest.

Version of Record: A version of this preprint was published at Communications Earth & Environment on May 10th, 2024. See the published version at <https://doi.org/10.1038/s43247-024-01425-4>.

Abstract

Two hyperthermal events with different carbon cycle perturbations occurred across the Cretaceous-Palaeogene (K-Pg) boundary, i.e., the late Maastrichtian Warming Event (LMWE) and the early Danian Dan-C2 event. However, the roles played by Deccan volcanism and orbital forcing in these two hyperthermals are still debated. Here, we obtain a new terrestrial $\delta^{13}\text{C}_{\text{carb}}$ record in the Nanxiong Basin (southeastern China) and compare it with marine records. The results show that both the LMWE and Dan-C2 event can be well distinguished in the terrestrial record and that the Dan-C2 event is characterized by a typical hyperthermal event; however, the specificity of the context under which this event occurred has resulted in inconsistencies in the marine records. In addition, the $\delta^{13}\text{C}$ excursion during the LMWE was more muted and prolonged than that during the Dan-C2 event, and the short-eccentricity cycle disappeared in the marine record during the LMWE, indicating that Deccan volcanism perturbed the carbon cycle during the LMWE, while the Dan-C2 event was less influenced by volcanic perturbation.

Introduction

A series of hyperthermal events characterized by transient warming and significant negative carbon isotope excursion (CIE) occurred during the late Cretaceous–early Palaeogene^{1,2}. Among them, the Late Maastrichtian Warming Event (LMWE) and the early Danian Dan-C2 event occurred across the Cretaceous-Palaeogene (K-Pg) boundary. Both were related to significant climatic and biotic changes; for instance, the LMWE was probably related to mass extinction at the end of the Cretaceous^{3–5}, while the Dan-C2 event promoted biotic recovery after the extinction^{4,6}.

The Dan-C2 event has been distinguished in the Atlantic Ocean^{1,6–9}, the Tethys Ocean^{10–12}, and the middle and lower latitudes of Eurasia^{4,13–16}. Compared to other hyperthermal events, the $\delta^{13}\text{C}$ negative excursions during the Dan-C2 event were restricted to planktonic foraminifera and bulk records in parts of the Atlantic and Tethys Oceans, while benthic foraminifera rarely recorded this event^{1,9}. Furthermore, the warming indicated by oxygen isotopes ($\delta^{18}\text{O}$) during this event was also limited to surface waters in parts of the North Atlantic, with evidence of warming in bottom waters generally lacking^{1,9,17} (supporting information Text S1, Fig. S1). Therefore, the global significance of the Dan-C2 event and even whether it should be regarded as a true hyperthermal are still controversial^{1,7,17}.

Two main sources of the massive ^{12}C -rich CO_2 triggering of the carbon cycle during the LMWE and Dan-C2 event were proposed: Deccan volcanism and carbon pools controlled by orbital forcing. The extremely negative values of the CIE for the LMWE and Dan-C2 event are located at the maxima of the 405-kyr long-eccentricity cycle^{18,4,12}. Moreover, the two CIEs of the Dan-C2 event correspond to two 100-kyr short-eccentricity maxima¹, indicating that orbital forcing contributed to the CIE during both the LMWE and the Dan-C2 event. The overlapping occurrences of Deccan volcanism and two hyperthermals suggest that the large amount of volcanic carbon emitted could have also played a role in driving

hyperthermals, especially the LMWE^{3,5,6,18}. However, this speculation is plausible and contemporaneous and lacks causal connection¹⁹. Recent modelling efforts to simulate CO₂ emission scenarios from Deccan volcanism have yielded conflicting results, with either more CO₂²⁰, half of the CO₂⁶, or one-third of the CO₂²¹ released before the K-Pg boundary. Therefore, the roles that Deccan volcanism played in perturbing the carbon cycle in the LMWE and the Dan-C2 event are still unclear.

To date, most of the carbon isotope records are from marine sediments, whereas terrestrial records are lacking. Our previous work showed that the LMWE and Dan-C2 event were recorded by red strata in the Nanxiong Basin (Southeastern China, Fig. 1). Hg and its isotopes indicate that they formed during Deccan volcanism; moreover, both hyperthermals were related to the 405-kyr long eccentricity cycle^{4,15,16}. However, due to the low resolution of the $\delta^{13}\text{C}_{\text{carb}}$ data, detailed comparisons with marine records and in-depth analyses of carbon cycle processes are limited. Here, a total of 274 fresh samples from the upper part of the Zhenshui Formation to the lower Xiahui part of the Shanghu Formation (Fig. 1b) were collected, then we obtain a new $\delta^{13}\text{C}_{\text{carb}}$ record across the K-Pg boundary in the basin and compare it with other published records to reveal 1) the terrestrial records of the LMWE and Dan-C2 event, as well as the global significance of the Dan-C2 event; and 2) the relative contributions of Deccan volcanism and orbital forcing to the carbon cycle during the two hyperthermal events.

Results

The $\delta^{13}\text{C}$ value of the bulk carbonate from the Nanxiong Basin (Fig. 2c) is consistent with the previous $\delta^{13}\text{C}$ values of pedogenic carbonate nodules that were not affected by diagenesis^{22,23}(Fig. S2a); moreover, there is no significant correlation between $\delta^{13}\text{C}_{\text{carb}}$ and $\delta^{18}\text{O}_{\text{carb}}$ (Fig. S2b), suggesting that the influence of diagenesis on our bulk carbonate $\delta^{13}\text{C}$ can be ruled out. $\delta^{13}\text{C}_{\text{carb}}$ shows a steady decrease from 66.4 to 66.2 Ma, reaches a minimum at approximately 66.2 Ma, with a negative CIE of $\sim 1.5\text{‰}$, and then slowly increases to the K-Pg boundary, corresponding to the LMWE. $\delta^{13}\text{C}_{\text{carb}}$ decreases sharply immediately after the K-Pg boundary and then shows an overall increase, with several negative excursions, such as the double CIEs at ~ 65.8 and ~ 65.7 Ma, which indicate that the Dan-C2 event characterized by the first CIE ($\sim 3\text{‰}$) was larger than the second CIE ($\sim 2\text{‰}$). In addition, another excursion of $\delta^{13}\text{C}_{\text{carb}}$ ($\sim 2\text{‰}$) occurred at ~ 65.3 Ma, which should correspond to the Lower C29n event. Overall, the $\delta^{13}\text{C}_{\text{carb}}$ values in the Nanxiong Basin can be well compared with the $\delta^{13}\text{C}_{\text{bulk}}$ values at ODP site 1262 (Fig. 2e); both show more muted CIEs during the LMWE than during the Dan-C2 event. In addition, the total duration of the onset, peak, and recovery of the LMWE ($\sim 200\text{--}300$ kyr) is significantly longer than that of each of the CIEs during the Dan-C2 event (~ 100 kyr) (Figs. 2c and 2e). However, the magnitudes of the CIEs in the Nanxiong Basin ($1.5\text{--}3\text{‰}$) are greater than those in ODP Site 1262 ($0.5\text{--}1\text{‰}$), which is also consistent with the findings of previous studies showing that the CIE magnitude is greater in the terrestrial record than in the marine record for the same hyperthermal event^{24,25}.

Evolutionary power spectral analysis revealed that both the $\delta^{13}\text{C}_{\text{carb}}$ of the Nanxiong Basin and the $\delta^{13}\text{C}_{\text{bulk}}$ of ODP site 1262 exhibited significant 405-kyr long eccentricity cycles from 66.6 to 65 Ma (Fig. 3a). The dramatic negative excursion of global $\delta^{13}\text{C}$ immediately after the K-Pg boundary was probably related to the large amount of CO_2 injected into the atmosphere by the Chicxulub impact³⁰, as well as the vital effects caused by mass extinction³¹. This dramatic excursion could lead to the insignificance of the 100-kyr short eccentricity cycle in both terrestrial and marine records under a 500 kyr sliding window during 66.2 to 65.8 Ma (Fig. 3a). To eliminate this bias, two discrete time windows without dramatic excursions were divided and then analysed separately with a sliding window of 150 kyr. The results reveal significant 100-kyr short eccentricity cycles both below and above the K-Pg boundary in the Nanxiong Basin (Fig. 3b); however, this cycle is complicated at ODP site 1262: the short eccentricity cycle was significant from 66.6 to 66.3 Ma, after which the significance level decreased and even disappeared from 66.2–66.0 Ma (Fig. 3c, right), after which the significance returned again after the K-Pg event (Fig. 3c, left).

Discussion

Was the Dan-C2 event a global hyperthermal event?

Our study provides a new terrestrial $\delta^{13}\text{C}$ record of the LMWE and Dan-C2 event, expanding their global distribution, especially the Dan-C2 event. However, there are still inconsistencies in marine records of the Dan-C2 event (supporting information, Text S1, Fig. S1), which are summarized in the following aspects: 1) the negative excursion of $\delta^{13}\text{C}$ is mainly recorded by bulk samples and planktonic foraminifera, while benthic foraminifera are rarely recorded; 2) the distribution is restricted to parts of the Atlantic Ocean and the Tethys Ocean; and 3) evidence of bottom-seawater warming is generally lacking.

To explore the possible reasons for the inconsistencies in the Dan-C2 event, we compared it to the Palaeocene-Eocene Thermal Maximum (PETM), which is the most studied hyperthermal event. The CIE of the PETM can reach 7‰ in terrestrial records and only 3‰ in marine records^{24,25,32}. Two mechanisms have been proposed: 1) marine CIE records are commonly truncated by carbonate dissolution, so the most extreme values are not represented, leading to an incomplete CIE^{32,33}; and 2) the terrestrial CIE is amplified by environmental changes and fractionation effects caused by photosynthesis in plants³⁴. A similar phenomenon is also shown with the Dan-C2 event. The CIEs of $\delta^{13}\text{C}_{\text{organic}}$ and $\delta^{13}\text{C}_{\text{carb}}$ in Boltysh crater (Fig. S1I) and the Nanxiong Basin (Fig. 1c) can reach $\sim 3.0\text{‰}$, whereas the marine CIEs are less than 1.5‰ (Fig. S1). Differences in the carbon isotope records during the PETM are not only manifested in marine and terrestrial records but also among different types of carbonate records (bulk samples, planktonic foraminifera, or benthic foraminifera) and even within the same type of carbonate but in different marine regions³³ (supporting information Fig. S3 and Fig. 4). Ocean acidification during the PETM led to carbonate dissolution and shoaling of the carbonate compensation depth (CCD), causing the sediments to be clay-rich. The thickness of the clay layer increases with

increasing palaeodepth^{32,33}, indicating enhanced carbonate dissolution. The CIEs of $\delta^{13}\text{C}_{\text{bulk}}$ and $\delta^{13}\text{C}_{\text{benthic}}$ have significant negative correlations with palaeodepth (Figs. 4a and 4b), suggesting that the dissolution of carbonate suppressed the amplitude of the CIE. In addition to carbonate dissolution, the sedimentation rate also affects the CIE. The CIEs of $\delta^{13}\text{C}_{\text{bulk}}$ and $\delta^{13}\text{C}_{\text{benthic}}$ have positive correlations with sediment thickness (Figs. 4c and 4d). The greater the sediment thickness is, the greater the sedimentation rate, the more complete the carbonate isotope record, and the greater the CIE. Similarly, for the Dan-C2 event, the CIEs of $\delta^{13}\text{C}_{\text{bulk}}$ show a significant negative correlation with palaeodepth (Fig. 4e) but a positive correlation with sediment thickness (Fig. 4f) and carbonate concentration (Fig. 4g), indicating that the CIEs of the Dan-C2 event are also influenced by the water depth, sedimentation rate, and carbonate dissolution, leading to some differences in the CIE records from different regions.

However, compared with the PETM, the Dan-C2 event was a short-lived and muted warming event that occurred under a specific environmental background, for instance, biotic turnover and drastic ecosystem changes caused by mass extinction. Under normal oceanic conditions, phytoplankton preferentially convert $^{12}\text{CO}_2$ into organic matter through photosynthesis (primary productivity), and then, ^{12}C -rich organic carbon is transported to the bottom water through a biological pump (export productivity), thus promoting carbon exchange between the surface and the deep ocean³⁵. After the K-Pg boundary, a collapse occurred in the surface-bottom $\delta^{13}\text{C}$ gradient³⁶, which was initially thought to reflect either a collapse in primary productivity (“Strangelove Ocean”³⁶) or export productivity (“Living Ocean”³⁷) after the mass extinction. However, benthic faunal records show a lack of significant extinction of phytoplankton-dependent benthic foraminifera and an increased food flux to the seafloor in the southeastern Atlantic Ocean and the Pacific Ocean³¹. In addition, biogenic barium records indicate geographic heterogeneity in export productivity, an increase in the central Pacific Ocean, no changes in upwelling or shelf Atlantic sites, and decreases in the northeast and southwest Atlantic Ocean, Southern Ocean, and Indian Ocean³⁸. Thus, the “Resilient Ocean” and “Heterogeneous Ocean” have been proposed to explain these phenomena³⁹.

The spatial heterogeneity of primary/export productivity could cause heterogeneous carbon cycling processes between the surface and deep ocean, leading to inconsistent marine $\delta^{13}\text{C}$ records from the Dan-C2 event. However, this heterogeneity was proposed to be due to the limited number of sites, which is insufficient to reveal a robust pattern, and the mechanism responsible for this heterogeneity is still unclear³⁸. The geographic location⁴⁰, circulation, nutrient runoff from land, and stratification³⁸ are potential drivers of the spatially heterogeneous ocean and inconsistent records of the Dan-C2 event. For example, ODP site 1049C is located at a productive coastal upwelling site⁴¹ in the western North Atlantic, where a great deal of terrestrial materials are transported by surface ocean currents⁴²; in addition, the export productivity is stable⁴³, leading to strong negative excursions from all $\delta^{13}\text{C}_{\text{bulk}}$, $\delta^{13}\text{C}_{\text{planktic}}$ and $\delta^{13}\text{C}_{\text{benthic}}$ (Fig. S1a), especially negative excursions from $\delta^{13}\text{C}_{\text{benthic}}$. Although increased

export productivity was recorded at ODP sites 1209 and 1210 in the Central Pacific Ocean^{24,38}, there are no records of Dan-C2 event, probably due to pelagic and oligotrophic environments, as well as the lack of nutrients from terrestrial sources. Evidently, the mass extinction and the dramatic changes it brought are the indispensable causes of the spatial heterogeneity of the Dan-C2 records, but proposing a reasonable model to explain this mechanism requires additional records in the future.

The roles of Deccan volcanism and orbital forcing in the carbon cycle

The large amount of CO₂ released by large igneous provinces (LIPs) can cause perturbations to the global carbon cycle. In addition to LIPs, other carbon pools, such as peat and methane hydrates, which are modulated by eccentricity forcing, could also contribute to the carbon cycle during hyperthermals. For instance, during eccentricity minima, seasonally uniform annual precipitation is more suitable for carbon burial, whereas during eccentricity maxima, short wet seasons and prolonged dry seasons caused by “monsoon-like” precipitation could promote carbon release². In addition, methane hydrates buried in the marine shelf become unstable and decompose in response to orbital-driven warming, leading to large quantities of light carbon being emitted to the atmosphere-ocean system, further perturbing the global carbon cycle⁴⁴. Previous work has shown that the total mercury (Hg) concentration in the Nanxiong Basin has been anomalous from 66.4 to 65.6 Ma (Fig. 2b); combined with Hg isotope data, Ma et al.⁴ attributed these anomalies to volcanism in the central Deccan Traps. Both the LMWE and the Dan-C2 event temporally overlapped with the central Deccan volcanism (Fig. 2). Moreover, the LMWE and Dan-C2 event occurred during the last 405-kyr long eccentricity of the Maastrichtian and the first 405-kyr long eccentricity of the Danian, respectively (Figs. 2c, 2d, and 2e), and their CIE maxima were all within the maxima of the 405-kyr eccentricity cycle¹². Moreover, 100-kyr short eccentricity cycles were significant in both terrestrial and marine records (except for the LMWE of ODP 1262; Fig. 3). These findings imply that both Deccan volcanism and orbital forcing contributed to the LMWE and Dan-C2 event.

However, there are noticeable differences between the LMWE and Dan-C2 event: 1) the magnitude of the CIE during the LMWE (~ 1.5‰ in the Nanxiong Basin, <0.5‰ in ODP 1262) is more muted than in the Dan-C2 event (2–3‰ in the Nanxiong Basin, 0.6‰ in ODP 1262); 2) the LMWE was characterized by both surface and deep sea warming^{1,18}, while the Dan-C2 event was characterized by surface ocean warming, accompanied by little appreciable deep sea warming; 3) each of the double CIEs of the Dan-C2 event corresponds to a maxima of the 100-kyr eccentricity cycle, while the total duration of the onset, peak and recovery of the LMWE (200 ~ 300 kyr) was significantly longer than each CIE of the Dan-C2 event (Fig. 2); 4) the short eccentricity cycles are significant during the Dan-C2 event, whereas they are insignificant and even disappear during the LMWE in the marine record (Fig. 3); and 5) although the CIE maxima of both the Dan-C2 and the LMWE were all within the maxima of the 405-kyr eccentricity cycle, the onset of the LMWE occurred at the minima of the 405-kyr eccentricity cycle^{12,18} (Figs. 2c and 2e).

These apparent differences suggest that Deccan volcanism and orbital forcing played different roles in driving the LMWE and Dan-C2 event, as well as in the global carbon cycle.

High-precision chronologies indicate that both the eruption rate and volume were low during the early stage of the central Deccan Traps^{26,27} (Fig. 2a). However, CO₂ release has the potential to decouple from rates of surface volcanism because large amounts of CO₂ can be released through passive degassing^{6,27}, especially from intrusive magmas²⁰. The reconstructed atmospheric CO₂ concentration based on the pedogenic carbonate nodules showed higher *p*CO₂ values during the LMWE than during the Dan-C2 event^{5,45} (Fig. S4), which is consistent with direct measurements of melt-inclusion CO₂ concentrations, suggesting that early Deccan magmas were enriched with more CO₂²⁰. Although the onset of the LMWE occurred at the minima of the 405-kyr eccentricity¹⁸ (Figs. 2c and 2e), several thousand Gt of carbon that degassed from the early Deccan magmas was sufficient to trigger the LMWE^{6,20}. The $\delta^{13}\text{C}$ composition of volcanic CO₂ ($\sim -5\text{‰}$ ⁴⁶) is much more positive than that of other sources, such as peat ($\delta^{13}\text{C} \approx -25\text{‰}$ ⁴⁷) and methane hydrates ($\delta^{13}\text{C} \approx -60\text{‰}$ ⁴⁸); therefore, the massive amount of volcanic CO₂ emitted through passive degassing of early Deccan magmas could have led to muted and prolonged $\delta^{13}\text{C}$ negative excursions during the LMWE (Fig. 2), as well as disruption of the short-eccentricity cycle in the oceanic record (Fig. 3c, right). Although passive degassing triggered the LMWE, whether the amount of released CO₂ was sufficient to cause $\sim 4^\circ\text{C}$ of warming is still debated^{19,20}. Notably, 405-kyr long eccentricity cycles were significant during the LMWE according to both terrestrial and marine records (Fig. 3a), and even 100-kyr short eccentricity cycles were significant according to the terrestrial record (Fig. 3b, right), suggesting that Deccan CO₂ outgassing likely enhanced the climate sensitivity to orbital forcing, leading to a global warming of $\sim 4^\circ\text{C}$ ^{12,20}. After the K-Pg boundary, with a decrease in CO₂ released from the Deccan magma^{20,27}, the carbon cycle was mainly controlled by orbitally driven carbon pools with more negative $\delta^{13}\text{C}$ values, leading to larger CIEs (Fig. 2) and significant short-eccentricity cycles in both terrestrial and marine records (Figs. 3b left and 3c left). Due to the decrease in CO₂ emissions, *p*CO₂ and its warming effects were muted during the Dan-C2 event. The above speculated release scenario of Deccan volcanic CO₂ was further substantiated by long-term ocean-atmosphere-sediment carbon cycle reservoir (LOSCAR)⁴⁹ model simulations, which showed that prior to the K-Pg boundary, more CO₂ was released through passive degassing²⁰ (intrusive:extrusive = 5:1) or that half of the CO₂ was released (50:50 outgassing scenario) but with a higher emission rate⁶. The greater volume and higher rate of CO₂ release before compared to after the K-Pg boundary confirm that Deccan volcanism likely contributed to both the LMWE and Dan-C2 event but contributed more to the LMWE.

In conclusion, we provide a new terrestrial $\delta^{13}\text{C}$ record of the LMWE and Dan-C2 event in low-latitude East Asia, which can be compared with marine records, further expanding the global distribution of these events. The inconsistency of marine records for the Dan-C2 event is related to the drastic ecosystem changes caused by mass extinction, especially in the heterogeneous ocean, while the specific

mechanism remains to be revealed by additional studies. We hypothesize that Deccan volcanism and orbital forcing played different roles in the carbon cycles during the LMWE and Dan-C2 event. Deccan volcanic CO₂ triggered the LMWE through passive degassing, disturbed the carbon cycle and amplified the sensitivity of the climate to orbital forcing, whereas the Dan-C2 event was mainly controlled by orbital forcing, with weakening of the volcanic perturbation.

Materials and Methods

The Nanxiong Basin is in southeastern China (Fig. 1a); it is elongated, with its axis oriented from northeast to southwest. Continuous red fluvial–lacustrine clastics spanning from the Upper Cretaceous to the lower Palaeocene are preserved in the basin. Extensive chronostratigraphic, stratigraphic, palaeontological, and palaeoclimatic works have been carried out in the CGD-CGY section (also called the Datang section)^{15,16,22,23}, which is dominated by muddy siltstone and silty mudstone with interbedded sandstone and conglomerate (Fig. 1b). Many fossils have been preserved, for instance, dinosaurs, dinosaur footprints, dinosaur eggs, and mammals. Various palaeosol layers with pedogenic carbonate formed on the red clastics²². Previous studies have shown that the palaeoclimate in this basin across the K-Pg boundary was mainly hot and (semi)arid; moreover, the climatic evolution was consistent with marine records^{4,15}. A total of 274 fresh samples from the upper part of the Zhenshui Formation to the lower Xiahui part of the Shanghu Formation (CGD section; Fig. 1b) were collected at approximately 1 m intervals. The chronology of the CGD section follows that of Ma et al.⁴ and is based on the palaeomagnetic framework of Clyde et al.²² combined with a chronological control point on the K-Pg boundary.

The carbon isotopic composition of the bulk carbonate was determined using a Thermo Fisher Isotope ratio mass spectrometer (Mat 253) coupled with a GasBench II at the Laboratory for Stable Isotope Geochemistry, Institute of Geology and Geophysics, IGCCAS, through the production of CO₂ after reaction with phosphoric acid. Acid digestion was performed in a GasBench II in continuous flow mode at a temperature of 72 ± 0.1°C and a reaction time of 60 min, through which the generated CO₂ was transferred by high-purity (99.999%) He carrier gas into the mass spectrometer. The standard deviation of δ¹³C values was calculated from replicate analyses of an internal laboratory calcite standard, which is better than 0.15‰. The measured δ¹³C values are reported relative to those of the Vienna Pee Dee Belemnite (V-PDB).

To determine the contribution of orbital forcing to the carbon cycle, evolutionary power spectra were generated through the δ¹³C records of both the Nanxiong Basin and ODP 1262 using Acycle software⁵⁰. In preparation for this analysis, the δ¹³C records were interpolated linearly at 5-kyr and 2-kyr intervals for the Nanxiong Basin and ODP 1262 records, respectively, and detrended using local regression smoothing (LOWESS). The fast Fourier transform (FFT) method was selected, and the sliding windows were 500 kyr and 150 kyr for the complete and discrete time windows, respectively.

Declarations

Competing interests:

The authors declare no competing interests.

Author contribution:

Mingming Ma and Xiuming Liu designed this study; Mingming Ma and Mengdi Wang carried them out; Huixin Huang conducted the time-series analyses; Mingming Ma prepared the manuscript with contributions from all co-authors.

Acknowledgement:

This research was supported by the National Natural Science Foundation of China (awards 42277440 and 42130507), and the IGCP Project 679.

References

1. Barnet, J. S. K. *et al.* A High-Fidelity Benthic Stable Isotope Record of Late Cretaceous–Early Eocene Climate Change and Carbon-Cycling. *Paleoceanogr. Paleoclimatology* 34, 672–691 (2019).
2. Zachos, J. C., Mccarren, H., Murphy, B., Röhl, U. & Westerhold, T. Tempo and scale of late Paleocene and early Eocene carbon isotope cycles: Implications for the origin of hyperthermals. *Earth Planet. Sci. Lett.* 299, 242–249 (2010).
3. Li, L. & Keller, G. Abrupt deep-sea warming at the end of the Cretaceous. *Geology* 26, 995–998 (1998).
4. Ma, M. *et al.* Deccan Traps Volcanism Implicated in the Extinction of Non-Avian Dinosaurs in Southeastern China. *Geophys. Res. Lett.* 49, e2022GL100342 (2022).
5. Zhang, L. *et al.* Deccan volcanism caused coupled pCO₂ and terrestrial temperature rises, and pre-impact extinctions in northern China. *Geology* 46, 271–274 (2018).
6. Hull, P. M. *et al.* On impact and volcanism across the Cretaceous-Paleogene boundary. *Science* 367, 266–272 (2020).
7. Arreguín-Rodríguez, G. J. *et al.* Benthic foraminiferal turnover across the Dan-C2 event in the eastern South Atlantic Ocean (ODP Site 1262). *Palaeogeogr. Palaeoclimatol. Palaeoecol.* 572, 110410 (2021).
8. Krahl, G. *et al.* Environmental changes occurred during the Early Danian at the Rio Grande Rise, South Atlantic Ocean. *Glob. Planet. Change* 191, 103197 (2020).

9. Quillévéré, F., Norris, R. D., Kroon, D. & Wilson, P. A. Transient ocean warming and shifts in carbon reservoirs during the early Danian. *Earth Planet. Sci. Lett.* 265, 600–615 (2008).
10. Coccioni, R. *et al.* The Dan-C2 hyperthermal event at Gubbio (Italy): Global implications, environmental effects, and cause(s). *Earth Planet. Sci. Lett.* 297, 298–305 (2010).
11. Gilabert, V., Batenburg, S. J., Arenillas, I. & Arz, J. A. Contribution of orbital forcing and Deccan volcanism to global climatic and biotic changes across the Cretaceous-Paleogene boundary at Zumaia, Spain. *Geology* 50, 21–25 (2022).
12. Gilabert, V., Arenillas, I., Arz, J. A., Batenburg, S. J. & Robinson, S. A. Multiproxy analysis of paleoenvironmental, paleoclimatic and paleoceanographic changes during the early Danian in the Caravaca section (Spain). *Palaeogeogr. Palaeoclimatol. Palaeoecol.* 576, 110513 (2021).
13. Gilmour, I. *et al.* A high-resolution nonmarine record of an early Danian hyperthermal event, Boltysch crater, Ukraine. *Geology* 41, 783–786 (2013).
14. Jolley, D. W., Gilmour, I., Gilmour, M., Kemp, D. B. & Kelley, S. P. Long-term resilience decline in plant ecosystems across the danian dan-c2 hyperthermal event, boltysch crater, ukraine. *J. Geol. Soc.* 172, 491–498 (2015).
15. Ma, M., He, M., Zhao, M., Peng, C. & Liu, X. Evolution of atmospheric circulation across the Cretaceous–Paleogene (K–Pg) boundary interval in low-latitude East Asia. *Glob. Planet. Change* 199, 103435 (2021).
16. Zhao, M., Ma, M., He, M., Qiu, Y. & Liu, X. Evaluation of the four potential Cretaceous-Paleogene (K–Pg) boundaries in the Nanxiong Basin based on evidences from volcanic activity and paleoclimatic evolution. *Sci. China Earth Sci.* 64, 631–641 (2021).
17. Westerhold, T., Röhl, U., Donner, B., McCarren, H. K. & Zachos, J. C. A complete high-resolution Paleocene benthic stable isotope record for the central Pacific (ODP Site 1209). *Paleoceanography* 26, PA002092 (2011).
18. Barnet, J. S. K., Littler, K., Kroon, D., Leng, M. J. & Zachos, J. C. A new high-resolution chronology for the late Maastrichtian warming event: Establishing robust temporal links with the onset of Deccan volcanism. *Geology* 46, 147–150 (2017).
19. Tobin, T. S., Bitz, C. M. & Archer, D. Modeling climatic effects of carbon dioxide emissions from Deccan Traps volcanic eruptions around the Cretaceous–Paleogene boundary. *Palaeogeogr. Palaeoclimatol. Palaeoecol.* 478, 139–148 (2017).
20. Nava, A. H. *et al.* Reconciling early Deccan Traps CO₂ outgassing and pre-KPB global climate. *Proc. Natl. Acad. Sci.* 118, e2007797118 (2021).
21. Cox, A. A. & Keller, C. B. A Bayesian inversion for emissions and export productivity across the end-Cretaceous boundary. *Science* 381, 1446–1451 (2023).
22. Clyde, W. C. *et al.* New Paleomagnetic and Stable-Isotope Results from the Nanxiong Basin, China: Implications for the K/T Boundary and the Timing of Paleocene Mammalian Turnover. *J. Geol.* 118, 131–143 (2010).

23. Wang Y. Paleoclimate changes of the late Cretaceous-early Paleocene in the Nanxiong basin, south China (in Chinese with English abstract). (Nanjing University, Nangjing, 2012).
24. Abels, H. A. *et al.* Terrestrial carbon isotope excursions and biotic change during Palaeogene hyperthermals. *Nat. Geosci.* 5, 326–329 (2012).
25. Chen, Z. *et al.* Structure of the carbon isotope excursion in a high-resolution lacustrine Paleocene–Eocene Thermal Maximum record from central China. *Earth Planet. Sci. Lett.* 408, 331–340 (2014).
26. Schoene, B. *et al.* U-Pb constraints on pulsed eruption of the Deccan Traps across the end-Cretaceous mass extinction. *Science* 363, 862–866 (2019).
27. Sprain, C. J. *et al.* The eruptive tempo of Deccan volcanism in relation to the Cretaceous-Paleogene boundary. *Science* 363, 866–870 (2019).
28. Laskar, J., Fienga, A., Gastineau, M. & Manche, H. La2010: a new orbital solution for the long-term motion of the Earth. *Astron. Astrophys.* 532, 784–785 (2011).
29. Kroon, D. & Zachos, J. C. Leg 208 synthesis: cenozoic climate cycles and excursions. *Sci. Results* 208, 1–55 (2007).
30. Artemieva, N., Morgan, J., & Expedition 364 Science Party. Quantifying the Release of Climate-Active Gases by Large Meteorite Impacts With a Case Study of Chicxulub. *Geophys. Res. Lett.* 44, 10180–10188 (2017).
31. Alegret, L., Thomas, E. & Lohmann, K. C. End-Cretaceous marine mass extinction not caused by productivity collapse. *Proc. Natl. Acad. Sci. U.S.A.* 109, 728–32 (2012).
32. Zachos, J. C. *et al.* Rapid Acidification of the Ocean During the Paleocene-Eocene Thermal Maximum. *Science* 308, 1611–1615 (2005).
33. McCarren, H., Thomas, E., Hasegawa, T., Röhl, U. & Zachos, J. C. Depth dependency of the Paleocene-Eocene carbon isotope excursion: Paired benthic and terrestrial biomarker records (Ocean Drilling Program Leg 208, Walvis Ridge). *Geochem. Geophys. Geosyst.* 9, Q10008 (2008).
34. Bowen, G. J., Beerling, D. J., Koch, P. L., Zachos, J. C. & Quattlebaum, T. A humid climate state during the Palaeocene/Eocene thermal maximum. *Nature* 432, 495–499 (2004).
35. Hilting, A. K., Kump, L. R. & Bralower, T. J. Variations in the oceanic vertical carbon isotope gradient and their implications for the Paleocene-Eocene biological pump. *Paleoceanogr. Paleoclimatology* 23, PA3222 (2008).
36. Hsü, K. J. *et al.* Environmental and evolutionary consequences of mass-mortality at the end of the Cretaceous. *Science* 216, 249–256 (1982).
37. D'Hondt, S. Consequences of the Cretaceous/Paleogene mass extinction for marine ecosystems. *Annu. Rev. Ecol. Evol. Syst.* 36, 295–317 (2005).
38. Hull, P. M. & Norris, R. D. Diverse patterns of ocean export productivity change across the Cretaceous-Paleogene boundary: New insights from biogenic barium. *Paleoceanography* 26, PA3205 (2011).

39. Esmeray-Senlet, S. *et al.* Evidence for reduced export productivity following the Cretaceous/Paleogene mass extinction. *Paleoceanography* 30, 718–738 (2015).
40. Jiang, S., Bralower, T. J., Patzkowsky, M. E., Kump, L. R. & Schueth, J. D. Geographic controls on nanoplankton extinction across the Cretaceous/Palaeogene boundary. *Nat. Geosci.* 3, 280–285 (2010).
41. Alegret, L. & Thomas, E. Cretaceous/Paleogene boundary bathyal paleo-environments in the central North Pacific (DSDP Site 465), the Northwestern Atlantic (ODP Site 1049), the Gulf of Mexico and the Tethys: The benthic foraminiferal record. *Palaeogeogr. Palaeoclimatol. Palaeoecol.* 224, 53–82 (2005).
42. Nauter-Alves, A. *et al.* Biotic turnover and carbon cycle dynamics in the early Danian event (Dan-C2): New insights from Blake Nose, North Atlantic. *Glob. Planet. Change* 221, 104046 (2023).
43. Faul, K. L., Anderson, L. D. & Delaney, M. L. Late Cretaceous and early Paleogene nutrient and paleoproductivity records from Blake Nose, western North Atlantic Ocean. *Paleoceanography* 18, PA000722 (2003).
44. Lunt, D. J. *et al.* A model for orbital pacing of methane hydrate destabilization during the Palaeogene. *Nat. Geosci.* 4, 775–778 (2011).
45. Nordt, L. C., Atchley, S. & Dworkin, S. Terrestrial evidence for two greenhouse events in the latest Cretaceous. *Geol. Soc. Am.* 13, 4–9 (2003).
46. Grard, A., Francois, L. M., Dessert, C., B. Dupré & Y. Godd ris. Basaltic volcanism and mass extinction at the Permo-Triassic boundary: Environmental impact and modeling of the global carbon cycle. *Earth Planet. Sci. Lett.* 234, 207–221 (2005).
47. DeConto, R. M. *et al.* Past extreme warming events linked to massive carbon release from thawing permafrost. *Nature* 484, 87–91 (2012).
48. Dickens, G. R., Castillo, M. M. & Walker, J. C. A blast of gas in the latest Paleocene: Simulating first-order effects of massive dissociation of oceanic methane hydrate. *Geology* 25, 259–262 (1997).
49. Zeebe, R. E. LOSCAR: Long-term Ocean-atmosphere-Sediment CARbon cycle Reservoir Model v2.0.4. *Geosci. Model Dev.* 5, 149–166 (2012).
50. Li, M., Hinnov, L. & Kump, L. Acycle: Time-series analysis software for paleoclimate research and education. *Comput. Geosci.* 127, 12–22 (2019).

Figures

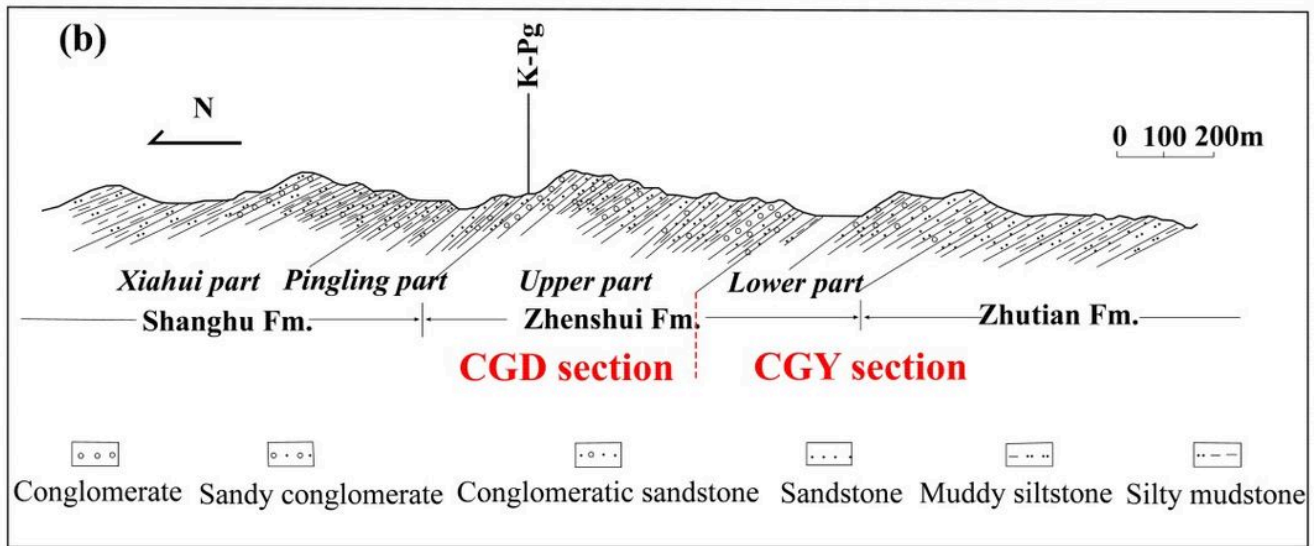
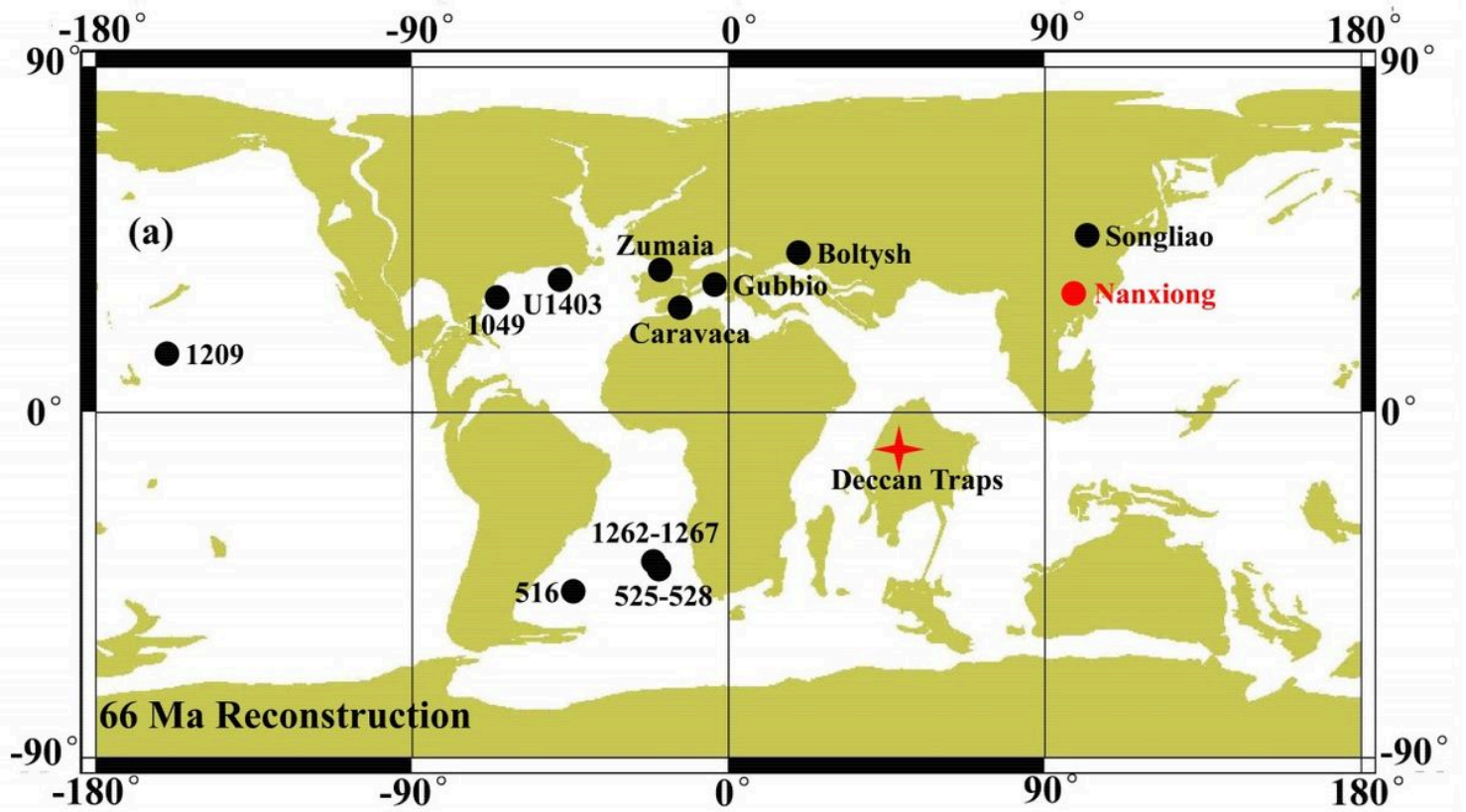


Figure 1

(a) Palaeogeographic reconstruction at 66 Ma (from the Ocean Drilling Stratigraphic Network Paleomap Project, <https://www.odsn.de/odsn/services/paleomap/paleomap.html>); the black dots indicate the studied sites of the Dan-C2 event; (b) stratigraphy of the CGD-CGY section in the Nanxiong Basin. CGD, Chinese–German Datang section; CGY, Chinese–German Yuanpu section.

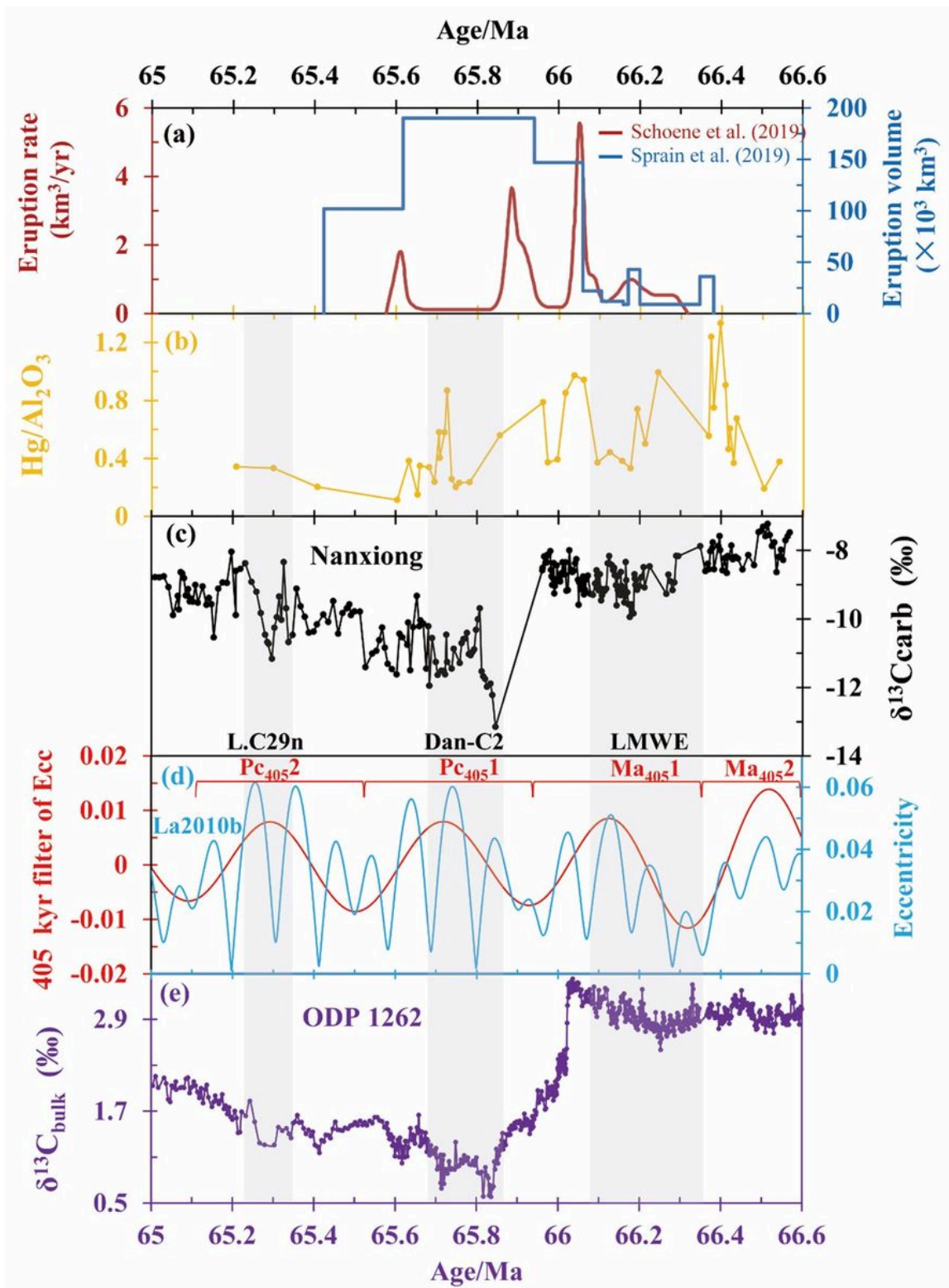


Figure 2

(a) Central Deccan eruption models based on the chronology of Schoene et al. (2019)²⁶ and Sprain et al. (2019)²⁷; (b) Hg/Al₂O₃ ratio of bulk samples from the Nanxiong Basin⁴; (c) δ¹³C record of carbonates in the Nanxiong Basin; (d) La2010b orbital solution (blue) filtered by long eccentricity (405-kyr), illustrated

in red²⁸; (e) $\delta^{13}\text{C}$ record of bulk samples from ODP 1262^{1,29}. LMWE: Late Maastrichtian Warming Event; Dan-C2: Dan-C2 event; L.C29n: Lower C29n event.

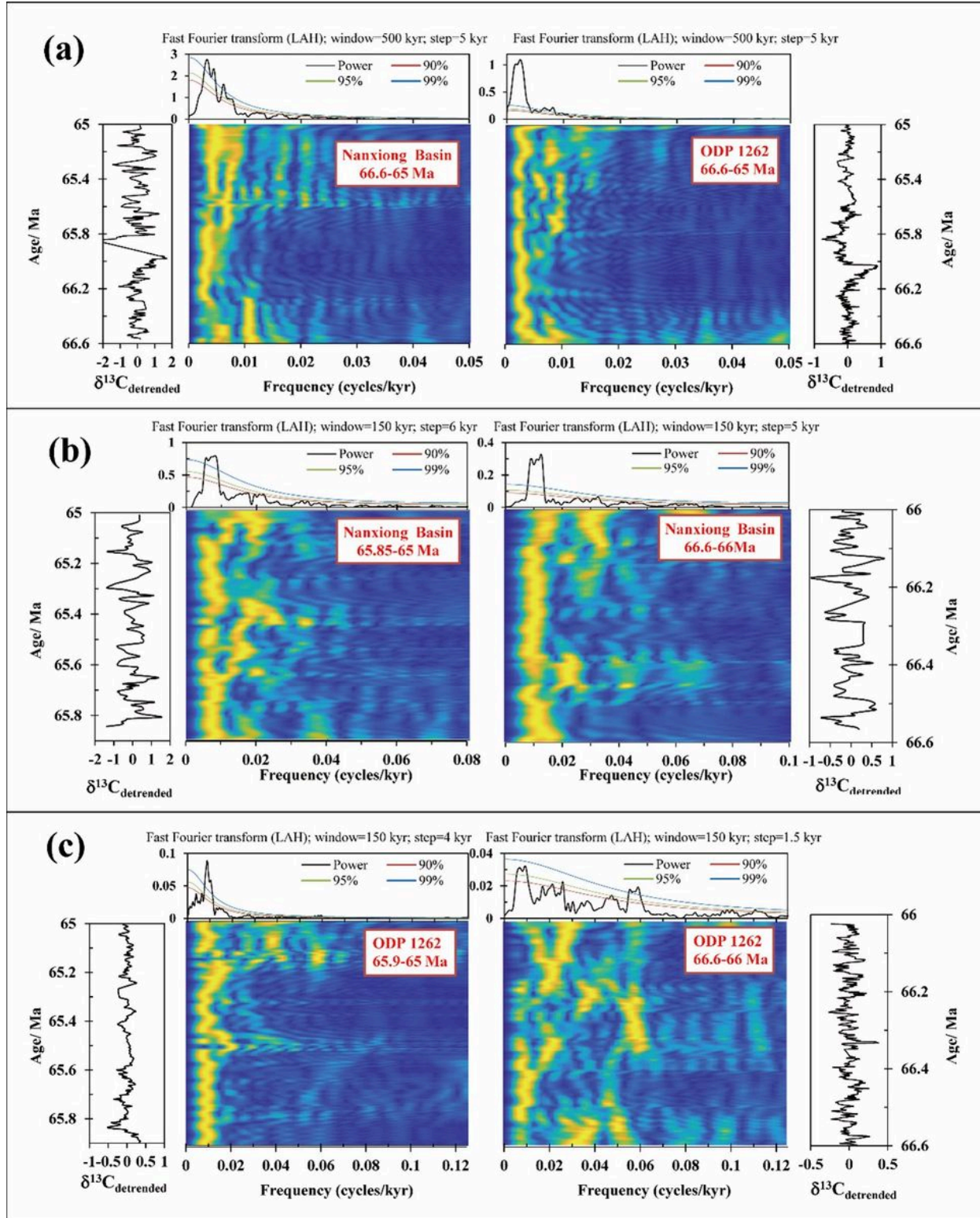


Figure 3

(a) Evolutionary power spectral analysis of the $\delta^{13}\text{C}_{\text{carb}}$ of Nanxiong Basin (left) and $\delta^{13}\text{C}_{\text{bulk}}$ of ODP 1262 (right) for the complete records; (b) evolutionary power spectral analysis of the $\delta^{13}\text{C}_{\text{carb}}$ from the

Nanxiong Basin for two discrete time windows: 65.85-65.0 Ma (left) and 66.6-66.0 Ma (right); (c) evolutionary power spectral analysis of the $\delta^{13}\text{C}_{\text{bulk}}$ of ODP 1262 for two discrete time windows: 65.9-65 Ma (left) and 66.6-66.0 Ma (right). Blue represents low spectral power, and yellow represents high spectral power.

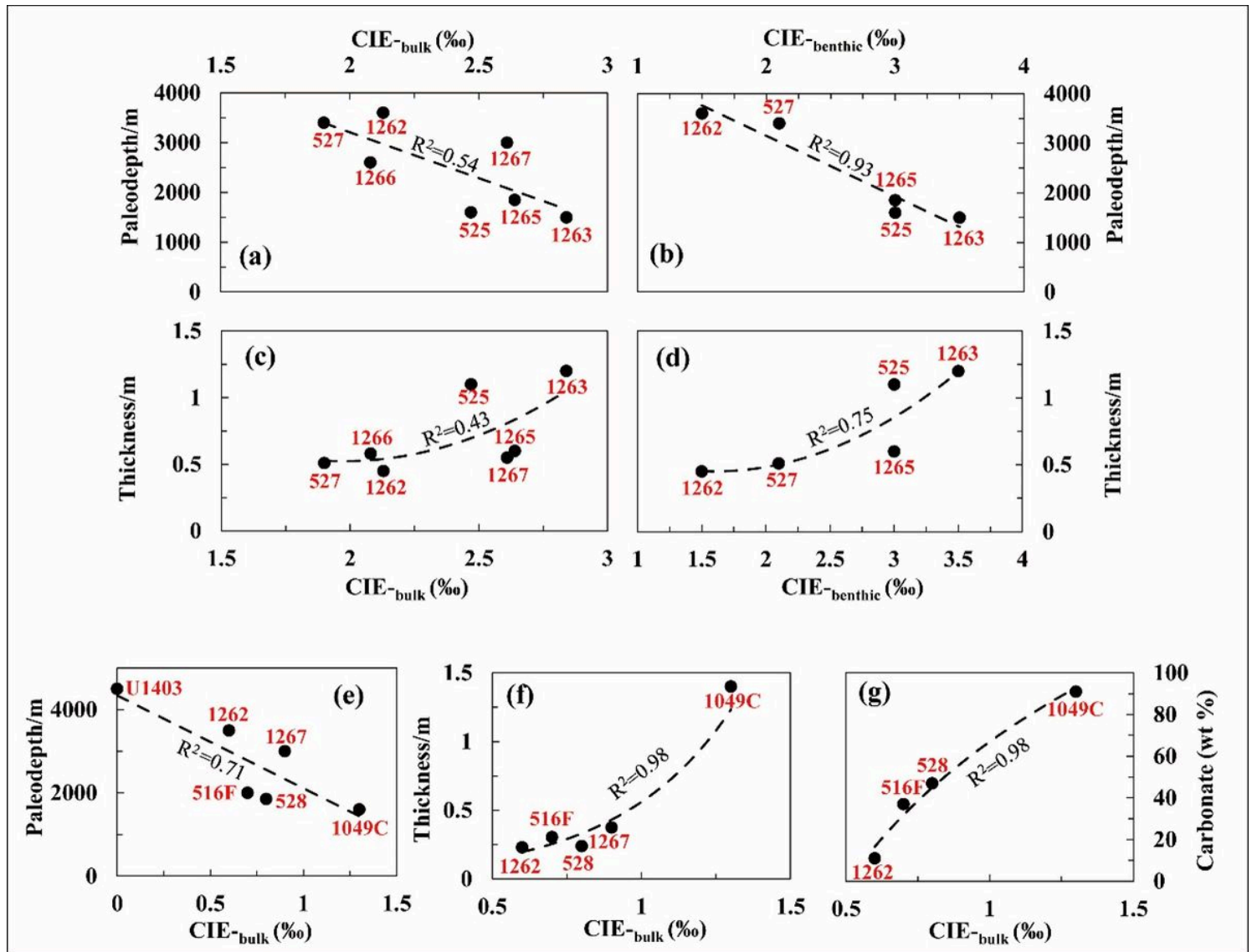


Figure 4

Scatter plots between the CIE and palaeodepth, sediment thickness, and carbonate concentration for the PETM (a-d) and the Dan-C2 event (e-g). The PETM data are from ODP 1262, ODP 1263, ODP 1265, ODP 1266, ODP 1267, DSDP 525, and DSDP 527. The Dan-C2 event data are from ODP 1049C, ODP 1262, ODP 1267, DSDP 516F, DSDP 528, and IODP U1403. More details are given in supporting information Tables S2 and S3.

Supplementary Files

This is a list of supplementary files associated with this preprint. Click to download.

- [Sl.docx](#)